A SIMPLE BUT EFFECTIVE AND EFFICIENT GLOBAL MODELING PARADIGM FOR IMAGE RESTORATION

Anonymous authors
Paper under double-blind review

ABSTRACT

Global modelling-based image restoration frameworks (*e.g.*, transformer-like architecture) have gained popularity. Despite the remarkable advancement, their success may be at the cost of model parameters and FLOPs while the intrinsic characteristics (*e.g.*, the task-specific degradation) are ignored. The objective of our work is orthogonal to previous studies and tailors a simple yet effective and efficient global modelling paradigm for image restoration. The key insights which motivate our study are two-fold: 1) Fourier transform is capable of disentangling image degradation and content component, serving as the image degradation prior embedded into image restoration framework; 2) Fourier domain innately embraces global property where each pixel of Fourier space is involved with all spatial pixels. We obey the de facto global modeling rule "spatial interaction + channel evolution" of previous studies. Differently, we customize the core designs: Fourier spatial interaction modeling and Fourier channel evolution. Equipped with the above-mentioned designs, our image restoration paradigm is verified on mainstream image restoration tasks including image de-raining, image enhancement, image de-hazing, and guided image super-resolution. Extensive experiments suggest that our paradigm achieves the competitive performance with fewer computational resources. Our main focus is not to beat previous frameworks but provide an alternative global modeling-based customized image restoration framework with efficient structure. Code will be publicly available.

1 INTRODUCTION

Image restoration aims to recover the latent clear image from its given degraded version. It is a highly ill-posed and challenging issue as there exists infinite feasible results for single degraded image. The representative image restoration tasks include image de-raining, image de-hazing, low-light enhancement, guided image super-resolution, etc.

In the past decades, a mount of research efforts have been devoted to solving the single image restoration problem, which can be classified into two categories: traditional optimization methods and deep learning-based methods (Zhang et al., 2018; Ren et al., 2018; Zhang et al., 2018; Ren et al., 2016b; Fu et al., 2021; Zhang et al., 2020; Liu et al., 2021a). In terms of traditional image restoration methods, they formulate the image restoration process as an optimization problem and develop various image priors of the expected latent clear image to constrain the solution space, *e.g.*, dark channel prior for image de-hazing (Dark, 2009), histogram distribution prior for underwater image enhancement (Li et al., 2016), non-local mean prior for image de-noising (Dixit & Phadke, 2013), sparse image prior for guided image super-resolution (Kim & Kwon, 2010) as well as the commonly-used local and non-local smooth prior (Chen et al., 2013), low-rank prior (Ren et al., 2016a). However, aforementioned image priors are difficult to develop and these traditional methods involve the iteration optimization, thus consuming the huge computational resources and further hindering their usage. In a word, the common sense is to explore the potential image prior to relieve the optimization difficulty of the ill-posed image restoration.

On the line of deep learning-based methods, convolutional neural networks (CNNs) have received widespread attention and achieved promising improvement in image restoration tasks over traditional methods (Liu et al., 2020; Ma et al., 2021; Zhang et al., 2021a; Zhou et al., 2021; 2022b). More recently, transformer and multi-layer perceptrons (MLPs)-based global modeling paradigms

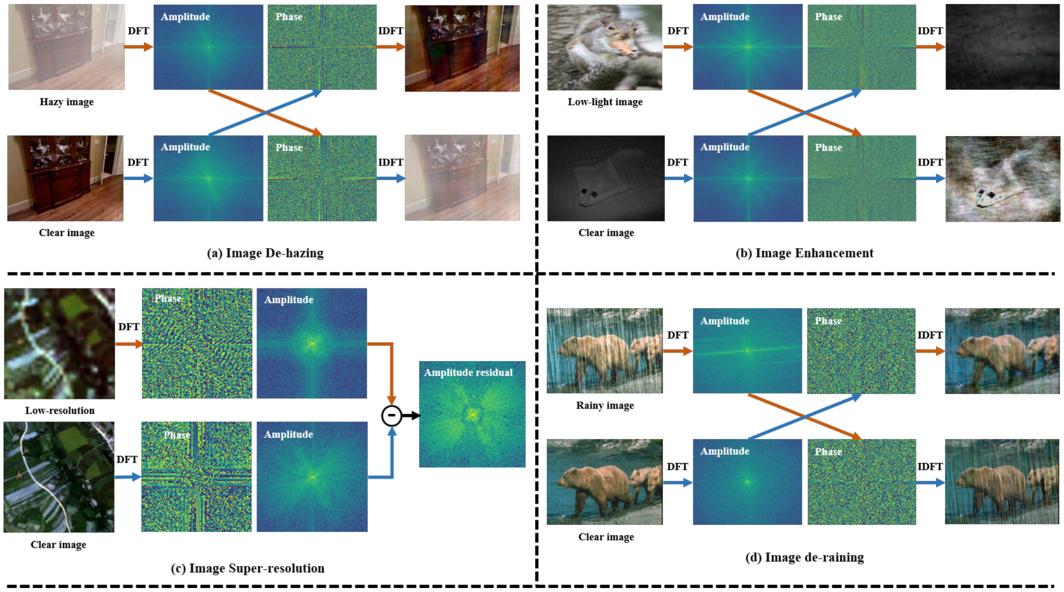

(a) Image De-hazing

(b) Image Enhancement

(c) Image Super-resolution

(d) Image de-raining

Figure 1: Motivations. Analysis of discrete Fourier transform (DFT) over mainstream image restoration tasks. In (a) and (d), we respectively swap the amplitude component and phase component of a degraded image and its clear version. It can be observed that the degradation effect is transferred, thus indicating that Fourier transform is capable of disentangling image degradation and content component and the degradation mainly lies in the amplitude component. To further verify our observation, we also swap the amplitude component and phase component of a degraded image and an irrelevant image in (b). The degradation is still mainly related to the amplitude component, such as the darkness for image enhancement. Similarly, a low-resolution image and its high-resolution counterpart are different in the amplitude component in (c). These observation motivates us to leverage the Fourier transform as the image degradation prior embedded into image restoration framework. More analysis and results can be found in the Appendix.

have struck the image restoration field and significantly surpassed the CNN-based methods. Despite the remarkable advancement, they are arbitrarily used for image restoration tasks while ignoring the intrinsic characteristics of specific image restoration task. The success may be owing to the huge cost of computational resources, limiting their practical applications, especially on resource-limited devices. We therefore wonder "Can we provide a customized global modeling image restoration paradigm in a simple but effective and efficient manner?"

To this end, motivated by our observations on Fourier transformation for image restoration tasks in Figure 1, we tailor a simple yet effective and efficient global modelling paradigm, which is orthogonal to previous studies and customized for image restoration. The core insights of our work are two-folder: 1) **general image restoration prior**: Fourier transform is capable of disentangling image degradation and content component, serving as the image degradation prior embedded into image restoration framework; 2) **global modeling**: Fourier domain innately embraces global property where each pixel of Fourier space is involved with all spatial pixels. As shown in Figure 2, the existing global modeling paradigm (*e.g.*, transformer and MLP-Mixer) follow the the de-facto global modeling rule "spatial interaction + channel evolution". Similarly, we obey the rule and customize the core designs: **Fourier spatial interaction and Fourier channel evolution**. Such designs are different from previous works and provide new insights on global modeling network structures for image restoration. Equipped with the above-mentioned designs, our image restoration paradigm tailed for image restoration is described in Figure 3. Extensive experiments are conducted on mainstream image restoration tasks including image de-raining, image enhancement, image de-hazing, and guided image super-resolution. Experimental results suggest that our paradigm achieves the competitive performance with fewer computational resources. To emphasize, *our main focus is not to beat previous frameworks but provide an alternative global modelling-based customized image restoration framework with efficient structure.*

Our contributions are summarized as follows: **(1)** We contribute the first global modeling paradigm for image restoration in a simple but effective and efficient manner. **(2)** We implicitly embed the

Fourier-based general image degradation prior into our core structures: Fourier spatial modeling and Fourier channel evolution, which provides new insights on the designs of global modeling-based image restoration network. **(3)** Our proposed paradigm achieves the competitive performance on several mainstream image restoration tasks with fewer computational resources.

2 Related Work

Image restoration. Image restoration aims to restore an image degraded by degradation factors (e.g. rain, haze, noise, lowlight) to a clear counterpart, which has been studied for a long time. Traditional image restoration methods are usually designed as an optimization problem, which incorporate specific priors of latent clear image to constrain the solution space (Dark, 2009; Li et al., 2016; Dixit & Phadke, 2013; Kim & Kwon, 2010). For example, dark channel prior (Dark, 2009) is proposed for image dehazing and histogram distribution prior (Li et al., 2016) is developed for underwater image enhancement. These methods involve iteration optimization, thus consuming the huge computational resources and limiting their application. Recently, deep learning-based methods have achieved impressive performance in a data-driven manner. Among them, most algorithms are designed with CNN-based architectures. Early works stack deep convolution layers for improving model representation ability, such as VDSR (Kim et al., 2016), DnCNN (Zhang et al., 2017), and ARCNN (Dong et al., 2015). Based on them, advanced methods have adopted more powerful architecture designs, such as residual block (Tai et al., 2017; Ehrlich & Davis, 2019) and dense block (Zhang et al., 2020; Dong et al., 2020). Besides, attention mechanisms (Zhang et al., 2018; 2021c) and multi-stage mechanism (Zamir et al., 2021; Chen et al., 2021c) have brought into image restoration algorithms that elevate the performance. However, the locality property of convolution operation limits the perception of global information that is critical for image restoration (Dixit & Phadke, 2013; Berman et al., 2016).

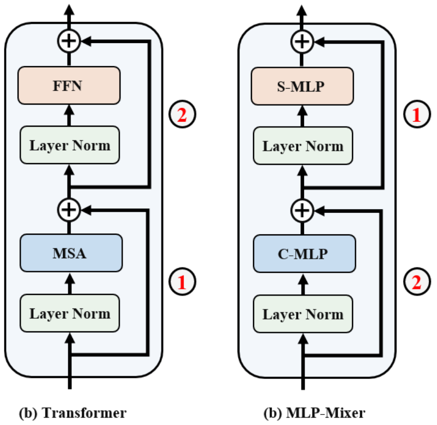

Figure 2: The underlying rule of existing global model paradigm: spatial interaction + channel evolution.

Global modeling. In recent years, global modeling techniques have gained much popularity in the computer vision community. A line of these methods is based on transformer (Vaswani et al., 2017), which has been adapted in numerous vision tasks such as vision recognition (Liu et al., 2021b; Xia et al., 2022) and segmentation (Chen et al., 2021b; Cao et al., 2021). Different from CNN-based architectures, transformer learns long-range dependencies between image patch sequences for global-aware modeling (Dosovitskiy et al., 2020). Due to its characteristic, various image restoration algorithms based on transformer have been proposed in recent years, which achieve superior performance in restoration tasks such as image image dehazing (Chun-Le Guo, 2022), image deraining (Xiao et al., 2022) and low-light image enhancement (Xu et al., 2022). Among them, a pioneer work IPT directly applies vanilla transformers to image patches (Chen et al., 2021a), while Uformer (Wang et al., 2022b) and SwinIR (Liang et al., 2021) apply efficient window-based local attention models on several image restoration tasks. However, the huge computation cost and parameters of transformer framework limit practical application. As another line of global modeling paradigm, multi-layer perceptrons (MLPs)-based methods have attracted attention in vision problems (Tolstikhin et al., 2021). To adapt this architecture for image restoration problems, MAXIM adopts a multi-axis MLP based mechanism to perceive information with global receptive field (Tu et al., 2022b). Nevertheless, it still costs enormous computation resources and is thus hard to apply in compact devices. In total, all above architectures are not fully to explore priors that are specific for image restoration tasks, which is important to lift performance. Recently, Fourier transformation has presented its effectiveness for global modeling (Chi et al., 2019; 2020). Instead of further exploring the efficacy of Fourier as global modeling in high-level tasks such as image classification, video action classification, human keypoint detection in (Chi et al., 2019), our work is the first to focus on the customized image restoration framework designs. The work proposed in (Chi et al., 2019) pays more attention to the global property while our framework further explores the intrinsic prior tailored for image restoration. In addition, different from existing Fourier techniques Chi et al. (2020) that emphasize the micro basic operator with the global receptive field, our work aims to focus on the macro framework design. In our work, we pay more attention to the customized image restoration global modeling framework. In this work, we investigate to incorporate restoration prior with Fourier transformation to conduct effective global modeling, which is efficient for practical application.

Different from existing transformer-based Wang et al. (2022a); Zamir et al. (2022) and MLP-based methods Tu et al. (2022a) that do not contain the intrinsic knowledge about image restoration tasks and only roughly focus on the global operator designs, our proposed framework is the first to explore the customized image restoration global modeling paradigm. Unlike these works that only consider global modeling, our work with efficient structure also meets the requirement of image restoration on edge devices with limited computation sources. In a word, our proposed framework incorporates both advantages of the global modeling mechanism and general image degradation prior that are introduced by Fourier transformation, thus achieving better performance.

3 Method

In this section, we first revisit the properties of Fourier transformation for image and then present an overview of the proposed global modeling paradigm, as illustrated in Figure 3. We further provide details of the fundamental building block of our method. Finally, we deep into the new loss functions proposed in our work.

3.1 Preliminary of Fourier transformation for image

As recognized, the Fourier transform is widely used to analyze the frequency content of images. For the images of multiple color channels, the Fourier transform is calculated and performed for each channel separately. For simplicity, we eliminate the notation of channels in formulas. Given an image $x \in R^{H \times W \times C}$, the Fourier transform $\mathcal{F}$ converts it to Fourier space as the complex component $\mathcal{F}(x)$, which is expressed as:

$$\mathcal{F}(x)(u,v) = \frac{1}{\sqrt{HW}} \sum_{h=0}^{H-1} \sum_{w=0}^{W-1} x(h,w) e^{-j2\pi(\frac{h}{H}u + \frac{w}{W}v)}, \tag{1}$$

$\mathcal{F}^{-1}(x)$ defines the inverse Fourier transform accordingly. Both the Fourier transform and its inverse procedure can be efficiently implemented by FFT/IFFT algorithms (Frigo & Johnson, 1998). The amplitude component $\mathcal{A}(x)(u,v)$ and phase component $\mathcal{P}(x)(u,v)$ are expressed as:

$$\begin{aligned} \mathcal{A}(x)(u,v)) &= \sqrt{R^2(x)(u,v)) + I^2(x)(u,v))}, \\ \mathcal{P}(x)(u,v)) &= \arctan[\frac{I(x)(u,v))}{R(x)(u,v))}], \end{aligned} \tag{2}$$

where $R(x)$ and $I(x)$ represent the real and imaginary part respectively. Note that the Fourier transformation and inverse procedure are computed independently on each channel of feature maps.

Targeting at image restoration, we employ Fourier transformation to conduct the detailed frequency analysis by revisiting the properties of phase and amplitude components, as shown in Figure 1. It can be observed that the degradation effect is transferred (mainly in the amplitude component) when swapping the amplitude component and phase component of a degraded image and its clear version. The phenomenon indicates that Fourier transform is capable of disentangling image degradation and content component and the degradation mainly lies in the amplitude component. This motivates us to leverage Fourier transform as the image degradation prior embedded into image restoration framework.

3.2 Framework

Structure flow. Our main goal is to develop a simple but effective and efficient global modeling paradigm for image restoration in a U-shaped hierarchical architecture, detailed in Figure 3. Given a

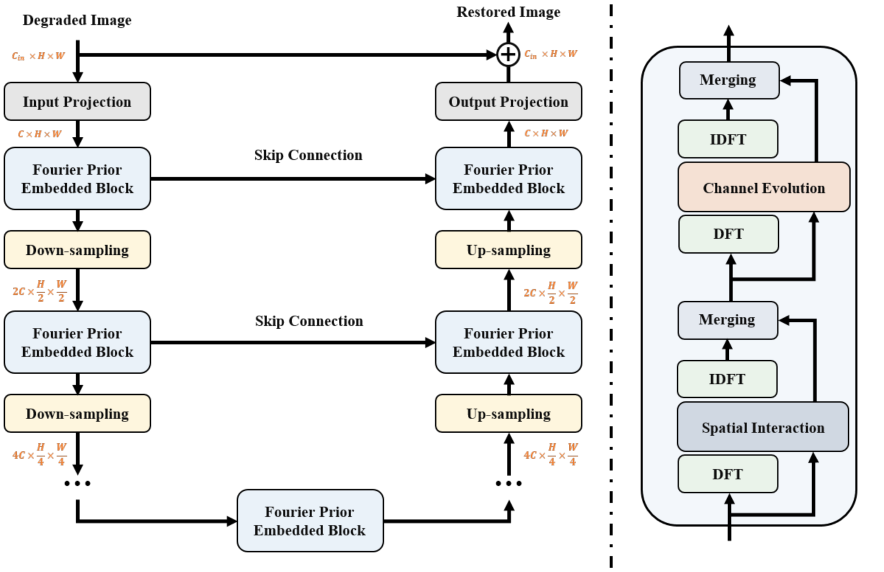
Degraded Image
Restored Image
$C_{in} \times H \times W$
$C_{in} \times H \times W$
Input Projection
Output Projection
$C \times H \times W$
$C \times H \times W$
Skip Connection
Fourier Prior Embedded Block
Fourier Prior Embedded Block
Down-sampling
Up-sampling
$2C \times \frac{H}{2} \times \frac{W}{2}$
$2C \times \frac{H}{2} \times \frac{W}{2}$
Skip Connection
Fourier Prior Embedded Block
Fourier Prior Embedded Block
Down-sampling
Up-sampling
$4C \times \frac{H}{4} \times \frac{W}{4}$
$4C \times \frac{H}{4} \times \frac{W}{4}$
Fourier Prior Embedded Block
Merging
IDFT
Channel Evolution
DFT
Merging
IDFT
Spatial Interaction
DFT

(b) Our proposed paradigm

(b) Fourier Prior Embedded Block

Figure 3: Overview of the proposed customized global modeling paradigm for image restoration.

degraded image $\mathbf{I} \in \mathrm{R}^{\mathrm{H} \times \mathrm{W} \times \mathrm{C_{in}}}$, the proposed paradigm first applies the convolution layer to project $\mathbf{I}$ into shallow feature embedding $\mathbf{X_0} \in \mathrm{R}^{\mathrm{H} \times \mathrm{W} \times \mathrm{C}}$. Next, following the U-shaped network designs, the obtained shallow embedding is passed through N encoder stages where each stage consists of a stack of the proposed core building module dubbed as Fourier Prior embedded Block and one downsampling layer. The Fourier Prior embedded Block takes advantage of the inborn global modeling property of Fourier transform, and obeys the underlying global modeling rule "spatial interaction + channel evolution" to customize the Fourier spatial and channel information interaction. In the downsampling layer, we downsample the 2D spatial feature maps using 3 × 3 convolution with stride 2. Similarly, in decoder stages, we employ the stack of the proposed Fourier Prior embedded Block and one upsampling layer for feature reconstruction in each stage. To assist the recovery process, each stage takes the high-level decoder features concatenated with the same stage low-level encoder features via skip connections as input. It is beneficial in preserving the fine structural and textural details in the restored images. Finally, a convolution layer is applied to the refined features to generate residual image $\mathbf{I} \in \mathrm{R}^{\mathrm{H} \times \mathrm{W} \times \mathrm{C_{in}}}$ to which degraded image is added to obtain the final restored image H_O.

Optimization flow. Besides the network designs for image restoration, we also introduce a new loss function to enable the network for better optimization, thus reconstructing the more pleasing results in both spatial and frequency domains. In detail, it consists of two parts: spatial domain loss and frequency domain loss. In contrast to existing methods that usually adopt pixel-level losses with local guidance in the spatial domain, we additionally propose the frequency domain supervision loss via Fourier transformation that is calculated on the global frequency components. Motivated by spectral convolution theorem, direct emphasis on the frequency content is capable of better reconstructing the global information, thus improving the restoration performance.

Let H_O and GT denote the network output and the corresponding ground truth respectively. We propose a joint spatial-frequency domain loss for supervising the network training. In spatial domain, we adopt $L1$ loss

$$\mathcal{L}_{spa} = \left\| H_O - GT \right\|_1 . \tag{3}$$

In frequency domain, we first employ DFT to convert H_O and GT into Fourier space where the amplitude and phase components are calculated. Then, the $L1$-norm of amplitude difference and phase difference between H_O and GT are summed to produce the total frequency loss

$$\mathcal{L}_{fre} = \left\| \mathcal{A}(H_O) - \mathcal{A}(GT) \right\|_1 + \left\| \mathcal{P}(H_O) - \mathcal{P}(GT) \right\|_1 . \tag{4}$$

Finally, the overall loss function is formulated as follows

$$\mathcal{L} = \mathcal{L}_{spa} + \lambda \mathcal{L}_{fre}, \tag{5}$$

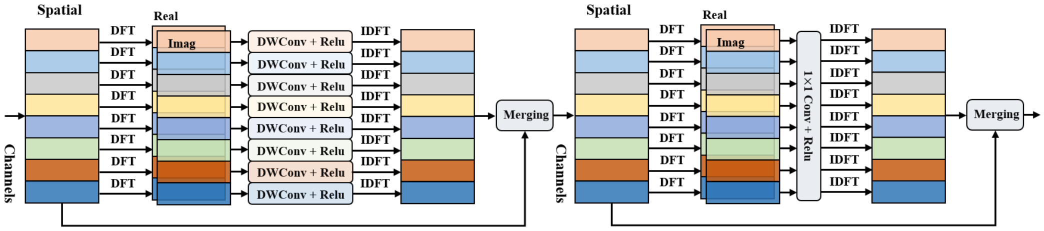

① Fourier spatial interaction ② Fourier channel evolution

Figure 4: Details of the Fourier Prior Embedded Block. Our block follows the global modeling rule "spatial interaction + channel evolution" but is with new designs: Fourier spatial interaction modeling and Fourier channel evolution.

where λ is weight factor and set to 0.1 empirically.

3.3 Fourier prior embedded block

As shown in Figure 4, the fundamental building block dubbed as Fourier prior embedded block contains two key elements: (a) Fourier spatial interaction, (b) Fourier channel evolution.

Fourier spatial interaction. In terms of the multi-channel feature maps, Fourier transformation is performed independently over each channel. Fourier prior embedded block takes the feature maps as input and then performs Fourier transformation to convert the spatial features into the real and imagery components. Suppose that the features denote as $\mathbf{X} \in \mathrm{R}^{\mathrm{H}\times\mathrm{W}\times\mathrm{B}}$, the corresponding Fourier transformation is expressed as

$$\mathrm{X}_{\mathrm{I}}^{(\mathrm{b})}, \mathrm{X}_{\mathrm{R}}^{(\mathrm{b})} = \mathcal{F}(\mathrm{X}^{(\mathrm{b})}), \tag{6}$$

where $\mathrm{b} = 1, \dots, \mathrm{B}$, $\mathrm{X}_{\mathrm{I}}^{(\mathrm{b})}$ and $\mathrm{X}_{\mathrm{R}}^{(\mathrm{b})}$ indicate the real and imagery respectively. Then we employ the spatial interaction by a stack of depth-wise convolution with kernel size of 3×3 and ReLU function. Specifically, $\mathrm{X}_{\mathrm{I}}^{(\mathrm{b})}$ and $\mathrm{X}_{\mathrm{R}}^{(\mathrm{b})}$ share the common depth-wise operator while different channels are independently performed. The spatial interaction can be written as follows:

$$S_I^{(b)} = \sigma\mathbf{DW}^{(\mathbf{b})}(X_I^{(b)}), \tag{7}$$

$$S_R^{(b)} = \sigma\mathbf{DW}^{(\mathbf{b})}(X_R^{(b)}), \tag{8}$$

where σ and DW indicate the ReLU function and depth-wise convolution respectively. Next, we apply the inverse DFT to transform the filtered frequency components of $S_I^{(b)}$ and $S_R^{(b)}$ back to spatial domain

$$X_S^b = F^{-1}(S_I^{(b)}, S_R^{(b)}). \tag{9}$$

According to spectral convolution theorem in Fourier theory, processing information in Fourier space is capable of capturing the global frequency representation in frequency domain. Finally, we merge the Fourier spatial interacted feature X_S by concatenating each component X_S^b with the spatial ones processed by the half-instance normalization block, thus generating the output S_X.

Fourier channel evolution. Followed by the spatial interaction, Fourier channel evolution aims to perform the point-wise channel interaction. Similarly, we first transform the previous step output S_X into the real and imagery components as C_R and C_I and then employ a stack of convolution operator with kernel size of 1×1 and ReLU function for channel interaction where each position in frequency space is shared. The channel interaction can be written as follows:

$$CX_I = \sigma\mathbf{conv}(cat[C_I^1, \dots, C_I^B]), \tag{10}$$

$$CX_R = \sigma\mathbf{conv}(cat[C_R^1, \dots, C_R^B]), \tag{11}$$

where conv indicates the convolution with kernel size of 1×1. Next, we apply the inverse DFT to transform the filtered frequency components of $CX_I^{(b)}$ and $CX_I^{(b)}$ back to spatial domain as

$$C_S^b = F^{-1}(CX_I^{(b)}, CX_R^{(b)}). \tag{12}$$

Finally, we perform the similar merging process with the first step, thus achieving the global modeling for both spatial and channel dimensions.

4 Experiment

To demonstrate the efficacy of our proposed customized image restoration paradigm, we conduct extensive experiments on multiple computer vision tasks, including image de-raining, image enhancement, image dehazing, and guided image super-resolution. More results can be found in the Appendix.

4.1 Experimental Settings

Low-light image enhancement. We evaluate our paradigm on two popular benchmarks, including LOL (Chen Wei, 2018) and Huawei (Hai et al., 2021). LOL dataset consists of 500 low-/normal- light image pairs, and we split 485 for training and 15 for testing. Huawei dataset contains 2480 paired images, and we split 2200 for training and 280 for testing. Further, we compared our paradigm with the following 13 state-of-the-art low-light image enhancement methods: SRIE (Fu et al., 2016), RetinexNet (Chen Wei, 2018), MBLLEN (Lv et al., 2018), EnlightenGAN (Jiang et al., 2021), GLADNet (Wang et al., 2018), Xu et al. (Xu et al., 2020), TBEFN (Lu & Zhang, 2020), KinD (Zhang et al., 2019), Zero-DCE++ (Li et al., 2021), DRBN (Yang et al., 2020), RetinexDIP (Zhao et al., 2021), RUAS (Liu et al., 2021a), KinD++ (Zhang et al., 2021b) and URetinex (Wu et al., 2022).

Image De-raining. Following the work (Zamir et al., 2021), our proposed paradigm is evaluated over 13,712 clean-rain image pairs, gathered from multiple synthetic datasets. With this single trained model, we perform evaluation on Rain100H and Rain100L. Further, we report the performance comparison between our designed paradigm and several representative state-of-the-art methods: DerainNet (Yang et al., 2017b), SEMI (Wei et al., 2019), DIDMDN (Zhang & Patel, 2018), UMRL (Yasarla & Patel, 2019), RESCAN (Li et al., 2018b), PReNet (Ren et al., 2019), MSPFN (Jiang et al., 2020), MPRNet (Zamir et al., 2021), HINet (Chen et al., 2021c).

Image Dehazing. We evaluate the proposed method on synthetic and real-world datasets. For synthetic scenes, we employ RESIDE (Li et al., 2018a) dataset. The subset Indoor Training Set (ITS) of RESIDE contains a total of 13990 hazy indoor images, generated from 1399 clear images. The subset Synthetic Objective Testing Set (SOTS) of RESIDE consists of 500 indoor hazy images and 500 outdoor ones. In addition, we adopt two real-world datasets: Dense-Haze (Ancuti et al., 2019) and NH-HAZE (Ancuti et al., 2020) to evaluate the generalization. Both of the two datasets consist of 55 paired images. We compare our paradigm with the promising methods: DCP (He et al., 2010) and DehazeNet (Cai et al., 2016), AOD-Net (Li et al., 2017), GridDehazeNet (Liu et al., 2019), FFA-Net (Qin et al., 2020), MSBDN (Dong et al., 2020) and AECR-Net (Wu et al., 2021).

Guided Image Super-resolution. Following (Zhou et al., 2022a; Yan et al., 2022), we adopt the pan-sharpening, the representative task of guided image super-resolution for evaluations. The WorldView II, WorldView III, and GaoFen2 in (Zhou et al., 2022a; Yan et al., 2022) are used. To verify the effectiveness of our paradigm, we choose the following representative pansharpening methods for comparison: 1) six state-of-the-art deep-learning based methods, including PNN (Masi et al., 2016), PANNET (Yang et al., 2017a), MSDCNN (Yuan et al., 2018), SRPPNN (Cai & Huang, 2021), GPPNN (Xu et al., 2021b) and INNformer(Zhou et al., 2022a); 2) five promising traditional methods, namely SFIM (Liu., 2000), Brovey (Gillespie et al., 1987), GS (Laben & Brower, 2000), IHS (Haydn et al., 1982), GFPCA (Liao et al., 2017).

Several widely-used image quality assessment (IQA) metrics are employed to evaluate the performance, including the relative dimensionless global error in synthesis (ERGAS) (Alparone et al., 2007), the peak signal-to-noise ratio (PSNR), Structural Similarity Index (SSIM), and the spectral angle mapper (SAM) (J. R. H. Yuhas & Boardman, 1992).

4.2 Comparison and Analysis

We perform quantitative performance comparison on the mainstream image restoration tasks in Table 1, Table 2, Table 3, and Table 4, where the best results are highlighted in bold. From the results, it can observed that our proposed paradigm achieves the competitively promising performance with fewer computational burden against the the baselines across all testing datasets on mainstream tasks, suggesting the effectiveness of our designs. For example, for the pan-sharpening, our paradigm obtains 0.17dB, 0.18dB, and 0.06dB PSNR gains than state-of-art method on the WorldView-II, WorldView-III and GaoFen2 datasets, respectively. In addition, in terms of image enhancement, our paradigm achieves the comparable results with the transformer-based SNRformer with the huge reduce of model parameters and FLOPs. The consistent conclusion can be found in other tasks.

Table 1: **Quantitative comparison of image de-hazing.**

Method	SOTS		Dense-Haze		NH-HAZE		Param (M)	GFLOPs
	PSNR	SSIM	PSNR	SSIM	PSNR	SSIM		
DCP	15.09	0.7649	10.06	0.3856	10.57	0.5196	-	-
DehazeNet	20.64	0.7995	13.84	0.4252	16.62	0.5238	0.01M	-
AOD-Net	19.82	0.8178	13.14	0.4144	15.40	0.5693	0.002M	0.1
GridDehazeNet	32.16	0.9836	13.31	0.3681	13.80	0.5370	0.96M	21.5
FFA-Net	36.39	0.9886	14.39	0.4524	19.87	0.6915	4.68M	288.1
MSBDN	33.79	0.9840	15.37	0.4858	19.23	0.7056	31.35M	41.5
KDDN	34.72	0.9845	14.28	0.4074	17.39	0.5897	5.99M	-
AECR-Net	37.17	0.9901	15.80	0.4660	19.88	0.7173	2.61M	43.0
Ours	**37.32**	**0.9901**	**15.95**	**0.4917**	**19.91**	**0.7214**	1.29M	20.6

Table 2: **Quantitative comparison of image de-raining.**

	Test100		Rain100H		Rain100L		Test1200		Param (M)	GFLOPs
Methods	PSNR↑	SSIM↑	PSNR↑	SSIM↑	PSNR↑	SSIM↑	PSNR↑	SSIM↑		
DerainNet	22.77	0.810	14.92	0.592	27.03	0.884	23.38	0.835	0.058M	1.453
SEMI	22.35	0.788	16.56	0.486	25.03	0.842	26.05	0.822	-	-
DIDMDN	22.56	0.818	17.35	0.524	25.23	0.741	29.65	0.901	0.373M	1.686
UMRL	24.41	0.829	26.01	0.832	29.18	0.923	30.55	0.910	0.98M	-
RESCAN	25.00	0.835	26.36	0.786	29.80	0.881	30.51	0.882	1.04M	20.361
PReNet	24.81	0.851	26.77	0.858	32.44	0.950	31.36	0.911	0.17M	73.021
MSPFN	27.50	0.876	28.66	0.860	32.40	0.933	32.39	0.916	13.22M	604.70
MPRNet	30.27	0.897	30.41	0.890	36.40	0.965	32.91	0.916	3.64M	141.28
HINet	30.29	0.906	30.65	0.894	37.28	0.970	33.05	0.919	3.72M	170.71
Ours	**30.54**	**0.911**	**30.76**	**0.896**	**37.47**	**0.970**	**33.05**	**0.921**	0.4M	16.753

Table 3: **Quantitative comparison of image enhancement.**

Method	LOL		Huawei		Param (M)	GFLOPs
	PSNR	SSIM	PSNR	SSIM		
SRIE	12.28	0.596	13.04	0.477	-	-
RobustRetinex	13.88	0.664	14.60	0.559	-	-
RetinexNet	16.77	0.425	16.65	0.485	0.84M	148.54
MBLLEN	17.56	0.729	16.63	0.526	0.45M	21.37
EnGAN	17.48	0.674	17.03	0.514	8.37M	72.61
GLADNet	19.72	0.680	17.76	0.521	1.13M	275.32
Xu	16.78	0.766	16.12	0.586	8.62M	68.45
TBEFN	17.35	0.781	16.88	0.575	0.49M	24.11
KinD	20.86	0.802	16.48	0.540	8.54M	36.57
ZeroDCE	15.29	0.518	12.46	0.407	0.08M	20.24
DRBN	20.13	0.801	18.46	**0.635**	0.58M	42.41
RUAS	16.41	0.500	13.76	0.516	0.003M	0.86
KinD++	21.30	0.822	15.78	0.452	8.28M	2970.50
URetinex	21.32	**0.835**	18.79	0.607	1.23M	68.37
Ours	**23.57**	0.832	**19.17**	0.621	0.08M	5.03

4.3 Ablation studies

To investigate the contribution of the key components, we have conducted comprehensive ablation studies on the WorldView-II satellite dataset of the Pan-sharpening task in terms of the number of network architecture stages and the frequency loss function. More ablated studies can be found in the Appendix.

Impact of the hierarchical number. To explore the impact of hierarchical number, i.e., the dom-sampling stages in our U-shape network, we experiment the proposed network with varying num-

Table 4: **Quantitative comparison of guided image super-resolution.**

c	worldview II				GaoFen2				worldview III				Param (M)	GFLOPs
Method	PSNR↑	SSIM↑	SAM↓	ERGAS↓	PSNR↑	SSIM↑	SAM↓	EGAS↓	PSNR↑	SSIM↑	SAM↓	EGAS↓		
SFIM	34.1297	0.8975	0.0439	2.3449	36.9060	0.8882	0.0318	1.7398	21.8212	0.5457	0.1208	8.9730	-	-
Brovey	35.8646	0.9216	0.0403	1.8238	37.7974	0.9026	0.0218	1.372	22.5060	0.5466	0.1159	8.2331	-	-
GS	35.6376	0.9176	0.0423	1.8774	37.2260	0.9034	0.0309	1.6736	22.5608	0.5470	0.1217	8.2433	-	-
IHS	35.2962	0.9027	0.0461	2.0278	38.1754	0.9100	0.0243	1.5336	22.5579	0.5354	0.1266	8.3616	-	-
GFPCA	34.5581	0.9038	0.0488	2.1411	37.9443	0.9204	0.0314	1.5604	22.3344	0.4826	0.1294	8.3964	-	-
PNN	40.7550	0.9624	0.0259	1.0646	43.1208	0.9704	0.0172	0.8528	29.9418	0.9121	0.0824	3.3206	0.689M	1.1289
PANNET	40.8176	0.9626	0.0257	1.0557	43.0659	0.9685	0.0178	0.8577	29.6840	0.9072	0.0851	3.4263	0.688M	1.1275
MSDCNN	41.3355	0.9664	0.0242	0.9940	45.6874	0.9827	0.0135	0.6389	30.3038	0.9184	0.0782	3.1884	2.39M	3.9158
SRPPNN	41.4538	0.9679	0.0233	0.9899	47.1998	0.9877	0.0106	0.5586	30.4346	0.9202	0.0770	3.1553	17.114M	21.1059
GPPNN	41.1622	0.9684	0.0244	1.0315	44.2145	0.9815	0.0137	0.7361	30.1785	0.9175	0.0776	3.2593	1.198M	1.3967
INNformer	41.6903	0.9704	0.0227	0.9514	47.3528	0.9893	0.0102	0.5479	30.5365	0.9225	0.0747	3.0997	0.706M	1.3907
Ours	**41.8325**	**0.9731**	**0.0219**	**0.9506**	**47.5334**	**0.9912**	**0.0102**	**0.5448**	**30.5987**	**0.9241**	**0.0738**	**3.0763**	0.715M	1.386

Table 5: **Ablation studies for hierarchical number.**

K	PSNR↑	SSIM↑	SAM↓	ERGAS↓
1	41.1827	0.9646	0.0255	1.0209
2	41.3324	0.9655	0.0249	1.0125
3	41.5331	0.9682	0.0240	0.9839
4	41.6867	0.9703	0.0235	0.9527

Table 6: **Ablation studies for frequency loss.**

Config	PSNR↑	SSIM↑	SAM↓	ERGAS↓
✗	41.7840	0.9725	0.0221	0.9508
✓	**41.8325**	**0.9731**	**0.0219**	**0.9506**

bers. The corresponding quantitative number K comparison from 1 to 4 is reported in Table 5. Observing the results from Table 5, it shows that the model performance can obtain considerable improvements at cost of computation (i.e., large hierarchical number)s. To balance the performance and computational complexity, we set $K = 4$ as default setting for pan-sharpening in this paper.

Effectiveness of the frequency loss. The new frequency loss aims to directly emphasize the global frequency information optimization. In Table 6, we remove it to examine its effectiveness. The results in Table 6 demonstrate that removing it severally degrades all metrics dramatically, indicating its significant role in our network.

5 LIMITATIONS

First, the more comprehensive experiments on broader computer vision tasks (*e.g.*, image de-noising and image de-blurring) have not been explored. Second, our proposed global modeling paradigm still follows the underlying rule "spatial interaction + channel evolution" of previous transformer-based or MLP-like architectures for general vision tasks. The de facto global modeling rule may be suboptimal for image restoration and it thus needs to be further investigated. In addition, our proposed paradigm has not achieved the best performance. Note that, the objective of our work is orthogonal to previous studies and we thus tailor a simple yet effective and efficient global modelling paradigm for image restoration. This work will spark further research to the realms of the customized global modeling image restoration framework, thus promoting practical application.

6 CONCLUSION

In this paper, we first propose a theoretically feasible global modeling paradigm for image restoration. We revisit the existing global modeling paradigm for general vision tasks and find the underlying design rule "spatial interaction + channel evolution". In addition, we revisit the inborn characteristics of Fourier prior for image restoration and find its prevailed decomposed property of image degradation and content component. Based on the above analysis, we customize the core designs: Fourier spatial modeling and Fourier channel evolution. Equipped with above designs, our image restoration paradigm is verified on mainstream image restoration tasks and achieves the competitive performance with fewer computational resources.

REFERENCES

L. Alparone, L. Wald, J. Chanussot, C. Thomas, P. Gamba, and L. M. Bruce. Comparison of pansharpening algorithms: Outcome of the 2006 grs-s data fusion contest. *IEEE Transactions on Geoscience and Remote Sensing*, 45(10):3012–3021, 2007.

Codruta O. Ancuti, Cosmin Ancuti, Mateu Sbert, and Radu Timofte. Dense haze: A benchmark for image dehazing with dense-haze and haze-free images. In *Proceedings of the IEEE International Conference on Image Processing*, pp. 1014–1018, 2019.

Codruta O Ancuti, Cosmin Ancuti, and Radu Timofte. NH-HAZE: An image dehazing benchmark with non-homogeneous hazy and haze-free images. In *Proceedings of the IEEE/CVF Conference on Computer Vision and Pattern Recognition Workshops*, pp. 444–445, 2020.

Dana Berman, Shai Avidan, et al. Non-local image dehazing. In *Proceedings of the IEEE Conference on Computer Vision and Pattern Recognition*, pp. 1674–1682, 2016.

Bolun Cai, Xiangmin Xu, Kui Jia, Chunmei Qing, and Dacheng Tao. DehazeNet: An end-to-end system for single image haze removal. *IEEE Transactions on Image Processing*, 25(11):5187–5198, 2016.

Jiajun Cai and Bo Huang. Super-resolution-guided progressive pansharpening based on a deep convolutional neural network. *IEEE Transactions on Geoscience and Remote Sensing*, 59(6): 5206–5220, 2021.

Hu Cao, Yueyue Wang, Joy Chen, Dongsheng Jiang, Xiaopeng Zhang, Qi Tian, and Manning Wang. Swin-unet: Unet-like pure transformer for medical image segmentation. *arXiv preprint arXiv:2105.05537*, 2021.

Hanting Chen, Yunhe Wang, Tianyu Guo, Chang Xu, Yiping Deng, Zhenhua Liu, Siwei Ma, Chunjing Xu, Chao Xu, and Wen Gao. Pre-trained image processing transformer. In *CVPR*, 2021a.

Jieneng Chen, Yongyi Lu, Qihang Yu, Xiangde Luo, Ehsan Adeli, Yan Wang, Le Lu, Alan L Yuille, and Yuyin Zhou. Transunet: Transformers make strong encoders for medical image segmentation. *arXiv preprint arXiv:2102.04306*, 2021b.

Liangyu Chen, Xin Lu, Jie Zhang, Xiaojie Chu, and Chengpeng Chen. HINet: Half instance normalization network for image restoration. In *Proceedings of the IEEE/CVF Conference on Computer Vision and Pattern Recognition*, pp. 182–192, 2021c.

Xiaowu Chen, Dongqing Zou, Steven Zhiying Zhou, Qinping Zhao, and Ping Tan. Image matting with local and nonlocal smooth priors. In *Proceedings of the IEEE conference on computer vision and pattern recognition*, pp. 1902–1907, 2013.

Wenhan Yang Jiaying Liu Chen Wei, Wenjing Wang. Deep retinex decomposition for low-light enhancement. In *British Machine Vision Conference*. British Machine Vision Association, 2018.

Lu Chi, Guiyu Tian, Yadong Mu, Lingxi Xie, and Qi Tian. Fast non-local neural networks with spectral residual learning. In *Proceedings of the 27th ACM International Conference on Multimedia*, pp. 2142–2151, 2019.

Lu Chi, Borui Jiang, and Yadong Mu. Fast fourier convolution. In H. Larochelle, M. Ranzato, R. Hadsell, M. F. Balcan, and H. Lin (eds.), *Advances in Neural Information Processing Systems*, 2020.

Saeed Anwar Runmin Cong Wenqi Ren Chongyi Li Chun-Le Guo, Qixin Yan. Image dehazing transformer with transmission-aware 3d position embedding. In *Proceedings of the IEEE/CVF Conference on Computer Vision and Pattern Recognition*, 2022.

Jifeng Dai, Min Shi, Weiyun Wang, Sitong Wu, Linjie Xing, Wenhai Wang, Xizhou Zhu, Lewei Lu, Jie Zhou, Xiaogang Wang, et al. Demystify transformers & convolutions in modern image deep networks. *arXiv preprint arXiv:2211.05781*, 2022.

Single Image Haze Removal Using Dark. Channel prior. kaiming he; jian sun; xiaoou tang. In *Computer Vision and Pattern Recognition*, 2009.

AA Dixit and AC Phadke. Image de-noising by non-local means algorithm. In *2013 International Conference on Signal Processing, Image Processing & Pattern Recognition*, pp. 275–277. IEEE, 2013.

Chao Dong, Yubin Deng, Chen Change Loy, and Xiaoou Tang. Compression artifacts reduction by a deep convolutional network. In *Proceedings of the IEEE international conference on computer vision*, pp. 576–584, 2015.

Hang Dong, Jinshan Pan, Lei Xiang, Zhe Hu, Xinyi Zhang, Fei Wang, and Ming-Hsuan Yang. Multi-scale boosted dehazing network with dense feature fusion. In *Proceedings of the IEEE/CVF Conference on Computer Vision and Pattern Recognition*, pp. 2157–2167, 2020.

Alexey Dosovitskiy, Lucas Beyer, Alexander Kolesnikov, Dirk Weissenborn, Xiaohua Zhai, Thomas Unterthiner, Mostafa Dehghani, Matthias Minderer, Georg Heigold, Sylvain Gelly, et al. An image is worth 16x16 words: Transformers for image recognition at scale. *arXiv preprint arXiv:2010.11929*, 2020.

Max Ehrlich and Larry S Davis. Deep residual learning in the jpeg transform domain. In *Proceedings of the IEEE/CVF International Conference on Computer Vision*, pp. 3484–3493, 2019.

M. Frigo and S. G. Johnson. Fftw: An adaptive software architecture for the fft. *Acoustics, Speech, and Signal Processing, 1988. ICASSP-88., 1988 International Conference on*, 3, 1998.

Xueyang Fu, Delu Zeng, Yue Huang, Xiao-Ping Zhang, and Xinghao Ding. A weighted variational model for simultaneous reflectance and illumination estimation. In *Proceedings of the IEEE Conference on Computer Vision and Pattern Recognition*, pp. 2782–2790, 2016.

Xueyang Fu, Zeyu Xiao, Gang Yang, Aiping Liu, Zhiwei Xiong, et al. Unfolding taylor's approximations for image restoration. *Advances in Neural Information Processing Systems*, 34: 18997–19009, 2021.

A. R. Gillespie, A. B. Kahle, and R. E. Walker. Color enhancement of highly correlated images. ii. channel ratio and ”chromaticity” transformation techniques - sciencedirect. *Remote Sensing of Environment*, 22(3):343–365, 1987.

Jiang Hai, Zhu Xuan, Ren Yang, Yutong Hao, Fengzhu Zou, Fang Lin, and Songchen Han. R2rnet: Low-light image enhancement via real-low to real-normal network. *arXiv preprint arXiv:2106.14501*, 2021.

R. Haydn, G. W. Dalke, J. Henkel, and J. E. Bare. Application of the ihs color transform to the processing of multisensor data and image enhancement. *National Academy of Sciences of the United States of America*, 79(13):571–577, 1982.

Kaiming He, Jian Sun, and Xiaoou Tang. Single image haze removal using dark channel prior. *IEEE Transactions on Pattern Analysis and Machine Intelligence*, 33(12):2341–2353, 2010.

A. F. Goetz J. R. H. Yuhas and J. M. Boardman. Discrimination among semi-arid landscape endmembers using the spectral angle mapper (sam) algorithm. *Proc. Summaries Annu. JPL Airborne Geosci. Workshop*, pp. 147–149, 1992.

Kui Jiang, Zhongyuan Wang, Peng Yi, Chen Chen, Baojin Huang, Yimin Luo, Jiayi Ma, and Junjun Jiang. Multi-scale progressive fusion network for single image deraining. In *CVPR*, pp. 8346–8355, 2020.

Yifan Jiang, Xinyu Gong, Ding Liu, Yu Cheng, Chen Fang, Xiaohui Shen, Jianchao Yang, Pan Zhou, and Zhangyang Wang. Enlightengan: Deep light enhancement without paired supervision. *IEEE Transactions on Image Processing*, 30:2340–2349, 2021.

Jiwon Kim, Jung Kwon Lee, and Kyoung Mu Lee. Accurate image super-resolution using very deep convolutional networks. In *Proceedings of the IEEE conference on computer vision and pattern recognition (CVPR)*, pp. 1646–1654, 2016.

Kwang In Kim and Younghee Kwon. Single-image super-resolution using sparse regression and natural image prior. *IEEE transactions on pattern analysis and machine intelligence*, 32(6):1127–1133, 2010.

C.A. Laben and B.V. Brower. Process for enhancing the spatial resolution of multispectral imagery using pan-sharpening. *US Patent 6011875A*, 2000.

Boyi Li, Xiulian Peng, Zhangyang Wang, Jizheng Xu, and Dan Feng. AOD-Net: All-in-one dehazing network. In *Proceedings of the IEEE International Conference on Computer Vision*, pp. 4770–4778, 2017.

Boyi Li, Wenqi Ren, Dengpan Fu, Dacheng Tao, Dan Feng, Wenjun Zeng, and Zhangyang Wang. Benchmarking single-image dehazing and beyond. *IEEE Transactions on Image Processing*, 28 (1):492–505, 2018a.

Chong-Yi Li, Ji-Chang Guo, Run-Min Cong, Yan-Wei Pang, and Bo Wang. Underwater image enhancement by dehazing with minimum information loss and histogram distribution prior. *IEEE Transactions on Image Processing*, 25(12):5664–5677, 2016.

Chongyi Li, Chunle Guo, and Change Loy Chen. Learning to enhance low-light image via zero-reference deep curve estimation. *IEEE Transactions on Pattern Analysis and Machine Intelligence*, 2021.

Xia Li, Jianlong Wu, Zhouchen Lin, Hong Liu, and Hongbin Zha. Recurrent squeeze-and-excitation context aggregation net for single image deraining. In *ECCV*, pp. 254–269, 2018b.

Jingyun Liang, Jiezhang Cao, Guolei Sun, Kai Zhang, Luc Van Gool, and Radu Timofte. Swinir: Image restoration using swin transformer. Proceedings of the IEEE/CVF International Conference on Computer Vision, pp. 1833–1844, 2021.

W. Liao, H. Xin, F. V. Coillie, G. Thoonen, and W. Philips. Two-stage fusion of thermal hyperspectral and visible rgb image by pca and guided filter. In *Workshop on Hyperspectral Image and Signal Processing: Evolution in Remote Sensing*, 2017.

J. G. Liu. Smoothing filter-based intensity modulation: A spectral preserve image fusion technique for improving spatial details. *International Journal of Remote Sensing*, 21(18):3461–3472, 2000.

Risheng Liu, Pan Mu, Xiaoming Yuan, Shangzhi Zeng, and Jin Zhang. A generic first-order algorithmic framework for bi-level programming beyond lower-level singleton. In *International Conference on Machine Learning*, pp. 6305–6315. PMLR, 2020.

Risheng Liu, Long Ma, Jiaao Zhang, Xin Fan, and Zhongxuan Luo. Retinex-inspired unrolling with cooperative prior architecture search for low-light image enhancement. In *Proceedings of the IEEE/CVF Conference on Computer Vision and Pattern Recognition*, pp. 10561–10570, 2021a.

Xiaohong Liu, Yongrui Ma, Zhihao Shi, and Jun Chen. GridDehazeNet: Attention-based multi-scale network for image dehazing. In *Proceedings of the IEEE/CVF International Conference on Computer Vision*, pp. 7314–7323, 2019.

Ze Liu, Yutong Lin, Yue Cao, Han Hu, Yixuan Wei, Zheng Zhang, Stephen Lin, and Baining Guo. Swin transformer: Hierarchical vision transformer using shifted windows. Proceedings of the IEEE/CVF International Conference on Computer Vision, pp. 10012–10022, 2021b.

Kun Lu and Lihong Zhang. Tbefn: A two-branch exposure-fusion network for low-light image enhancement. *IEEE Transactions on Multimedia*, 23:4093–4105, 2020.

Feifan Lv, Feng Lu, Jianhua Wu, and Chongsoon Lim. Mbllen: Low-light image/video enhancement using cnns. In *BMVC*, volume 220, pp. 4, 2018.

Long Ma, Risheng Liu, Jiaao Zhang, Xin Fan, and Zhongxuan Luo. Learning deep context-sensitive decomposition for low-light image enhancement. *IEEE Transactions on Neural Networks and Learning Systems*, 2021.

Giuseppe Masi, Davide Cozzolino, Luisa Verdoliva, and Giuseppe Scarpa. Pansharpening by convolutional neural networks. *Remote Sensing*, 8(7):594, 2016.

A. V. Oppenheim, G. Kopec, J. S. Lim, and S. C. Pohlig. Phase in speech and pictures. In *Acoustics, Speech, and Signal Processing, IEEE International Conference on ICASSP '79.*, 1979.

Xu Qin, Zhilin Wang, Yuanchao Bai, Xiaodong Xie, and Huizhu Jia. FFA-Net: Feature fusion attention network for single image dehazing. In *Proceedings of the AAAI Conference on Artificial Intelligence*, volume 34, pp. 11908–11915, 2020.

Dongwei Ren, Wangmeng Zuo, Qinghua Hu, Pengfei Zhu, and Deyu Meng. Progressive image deraining networks: A better and simpler baseline. In *CVPR*, pp. 3937–3946, 2019.

Wenqi Ren, Xiaochun Cao, Jinshan Pan, Xiaojie Guo, Wangmeng Zuo, and Ming-Hsuan Yang. Image deblurring via enhanced low-rank prior. *IEEE Transactions on Image Processing*, 25(7): 3426–3437, 2016a.

Wenqi Ren, Si Liu, Hua Zhang, Jinshan Pan, Xiaochun Cao, and Ming-Hsuan Yang. Single image dehazing via multi-scale convolutional neural networks. In *Proceedings of the European Conference on Computer Vision*, pp. 154–169. Springer, 2016b.

Wenqi Ren, Lin Ma, Jiawei Zhang, Jinshan Pan, Xiaochun Cao, Wei Liu, and Ming-Hsuan Yang. Gated fusion network for single image dehazing. In *Proceedings of the IEEE Conference on Computer Vision and Pattern Recognition*, pp. 3253–3261, 2018.

Ting Tai, Jian Yang, and Xiaoming Liu. Image super-resolution via deep recursive residual network. In *CVPR*, 2017.

Ilya O Tolstikhin, Neil Houlsby, Alexander Kolesnikov, Lucas Beyer, Xiaohua Zhai, Thomas Unterthiner, Jessica Yung, Andreas Steiner, Daniel Keysers, Jakob Uszkoreit, et al. Mlp-mixer: An all-mlp architecture for vision. *Advances in Neural Information Processing Systems*, 34:24261–24272, 2021.

Zhengzhong Tu, Hossein Talebi, Han Zhang, Feng Yang, Peyman Milanfar, Alan Bovik, and Yinxiao Li. Maxim: Multi-axis mlp for image processing. In *Proceedings of the IEEE/CVF Conference on Computer Vision and Pattern Recognition*, pp. 5769–5780, 2022a.

Zhengzhong Tu, Hossein Talebi, Han Zhang, Feng Yang, Peyman Milanfar, Alan Bovik, and Yinxiao Li. Maxim: Multi-axis mlp for image processing. In *Proceedings of the IEEE/CVF Conference on Computer Vision and Pattern Recognition*, pp. 5769–5780, 2022b.

Ashish Vaswani, Noam Shazeer, Niki Parmar, Jakob Uszkoreit, Llion Jones, Aidan N Gomez, Łukasz Kaiser, and Illia Polosukhin. Attention is all you need. *Advances in Neural Information Processing Systems*, 30, 2017.

Wenjing Wang, Chen Wei, Wenhan Yang, and Jiaying Liu. Gladnet: Low-light enhancement network with global awareness. In *2018 13th IEEE International Conference on Automatic Face & Gesture Recognition (FG 2018)*, pp. 751–755. IEEE, 2018.

Zhendong Wang, Xiaodong Cun, Jianmin Bao, Wengang Zhou, Jianzhuang Liu, and Houqiang Li. Uformer: A general u-shaped transformer for image restoration. In *Proceedings of the IEEE/CVF Conference on Computer Vision and Pattern Recognition*, pp. 17683–17693, 2022a.

Zhendong Wang, Xiaodong Cun, Jianmin Bao, Wengang Zhou, Jianzhuang Liu, and Houqiang Li. Uformer: A general u-shaped transformer for image restoration. In *CVPR*, 2022b.

Wei Wei, Deyu Meng, Qian Zhao, Zongben Xu, and Ying Wu. Semi-supervised transfer learning for image rain removal. In *CVPR*, pp. 3877–3886, 2019.

Haiyan Wu, Yanyun Qu, Shaohui Lin, Jian Zhou, Ruizhi Qiao, Zhizhong Zhang, Yuan Xie, and Lizhuang Ma. Contrastive learning for compact single image dehazing. In *Proceedings of the IEEE/CVF Conference on Computer Vision and Pattern Recognition*, pp. 10551–10560, 2021.

Wenhui Wu, Jian Weng, Pingping Zhang, Xu Wang, Wenhan Yang, and Jianmin Jiang. Uretinex-net: Retinex-based deep unfolding network for low-light image enhancement. In *Proceedings of the IEEE/CVF Conference on Computer Vision and Pattern Recognition (CVPR)*, pp. 5901–5910, June 2022.

Zhuofan Xia, Xuran Pan, Shiji Song, Li Erran Li, and Gao Huang. Vision transformer with deformable attention. In *Proceedings of the IEEE/CVF Conference on Computer Vision and Pattern Recognition*, pp. 4794–4803, 2022.

Jie Xiao, Xueyang Fu, Aiping Liu, Feng Wu, and Zheng-Jun Zha. Image de-raining transformer. *IEEE Transactions on Pattern Analysis and Machine Intelligence*, pp. 1–18, 2022. doi: 10.1109/TPAMI.2022.3183612.

Ke Xu, Xin Yang, Baocai Yin, and Rynson WH Lau. Learning to restore low-light images via decomposition-and-enhancement. In *Proceedings of the IEEE/CVF Conference on Computer Vision and Pattern Recognition*, pp. 2281–2290, 2020.

Qinwei Xu, Ruipeng Zhang, Ya Zhang, Yanfeng Wang, and Qi Tian. A fourier-based framework for domain generalization. In *CVPR*, pp. 14383–14392, 2021a.

Shuang Xu, Jiangshe Zhang, Zixiang Zhao, Kai Sun, Junmin Liu, and Chunxia Zhang. Deep gradient projection networks for pan-sharpening. In *IEEE Conference on Computer Vision and Pattern Recognition*, pp. 1366–1375, June 2021b.

Xiaogang Xu, Ruixing Wang, Chi-Wing Fu, and Jiaya Jia. Snr-aware low-light image enhancement. In *Proceedings of the IEEE/CVF Conference on Computer Vision and Pattern Recognition (CVPR)*, pp. 17714–17724, June 2022.

Keyu Yan, Man Zhou, Liu Liu, Chengjun Xie, and Danfeng Hong. When pansharpening meets graph convolution network and knowledge distillation. *IEEE Transactions on Geoscience and Remote Sensing*, 60:1–15, 2022. doi: 10.1109/TGRS.2022.3168192.

Junfeng Yang, Xueyang Fu, Yuwen Hu, Yue Huang, Xinghao Ding, and John Paisley. Pannet: A deep network architecture for pan-sharpening. In *IEEE International Conference on Computer Vision*, pp. 5449–5457, 2017a.

Wenhan Yang, Robby T Tan, Jiashi Feng, Jiaying Liu, Zongming Guo, and Shuicheng Yan. Deep joint rain detection and removal from a single image. In *CVPR*, pp. 1357–1366, 2017b.

Wenhan Yang, Shiqi Wang, Yuming Fang, Yue Wang, and Jiaying Liu. From fidelity to perceptual quality: A semi-supervised approach for low-light image enhancement. In *Proceedings of the IEEE/CVF Conference on Computer Vision and Pattern Recognition*, pp. 3063–3072, 2020.

Rajeev Yasarla and Vishal M Patel. Uncertainty guided multi-scale residual learning-using a cycle spinning cnn for single image de-raining. In *CVPR*, pp. 8405–8414, 2019.

Weihao Yu, Mi Luo, Pan Zhou, Chenyang Si, Yichen Zhou, Xinchao Wang, Jiashi Feng, and Shuicheng Yan. Metaformer is actually what you need for vision. In *Proceedings of the IEEE/CVF Conference on Computer Vision and Pattern Recognition*, pp. 10819–10829, 2022.

Q. Yuan, Y. Wei, X. Meng, H. Shen, and L. Zhang. A multiscale and multidepth convolutional neural network for remote sensing imagery pan-sharpening. *IEEE Journal of Selected Topics in Applied Earth Observations and Remote Sensing*, 11(3):978–989, 2018.

Syed Waqas Zamir, Aditya Arora, Salman Khan, Munawar Hayat, Fahad Shahbaz Khan, Ming-Hsuan Yang, and Ling Shao. Multi-stage progressive image restoration. In *Proceedings of the IEEE/CVF Conference on Computer Vision and Pattern Recognition*, pp. 14821–14831, 2021.

Syed Waqas Zamir, Aditya Arora, Salman Khan, Munawar Hayat, Fahad Shahbaz Khan, and Ming-Hsuan Yang. Restormer: Efficient transformer for high-resolution image restoration. In *Proceedings of the IEEE/CVF Conference on Computer Vision and Pattern Recognition*, pp. 5728–5739, 2022.

Hao Zhang, Han Xu, Xin Tian, Junjun Jiang, and Jiayi Ma. Image fusion meets deep learning: A survey and perspective. *Information Fusion*, 76:323–336, 2021a.

He Zhang and Vishal M Patel. Density-aware single image de-raining using a multi-stream dense network. In *Proceedings of the IEEE conference on computer vision and pattern recognition*, pp. 695–704, 2018.

Kai Zhang, Wangmeng Zuo, Yunjin Chen, Deyu Meng, and Lei Zhang. Beyond a gaussian denoiser: Residual learning of deep cnn for image denoising. *IEEE Transactions on Image Processing*, 26 (7):3142–3155, 2017.

Yonghua Zhang, Jiawan Zhang, and Xiaojie Guo. Kindling the darkness: A practical low-light image enhancer. In *Proceedings of the 27th ACM International Conference on Multimedia*, pp. 1632–1640, 2019.

Yonghua Zhang, Xiaojie Guo, Jiayi Ma, Wei Liu, and Jiawan Zhang. Beyond brightening low-light images. *International Journal of Computer Vision*, 129(4):1013–1037, 2021b.

Yulun Zhang, Kunpeng Li, Kai Li, Lichen Wang, Bineng Zhong, and Yun Fu. Image super-resolution using very deep residual channel attention networks. In *Proceedings of the European conference on computer vision (ECCV)*, pp. 286–301, 2018.

Yulun Zhang, Yapeng Tian, Yu Kong, Bineng Zhong, and Yun Fu. Residual dense network for image restoration. *IEEE Transactions on Pattern Analysis and Machine Intelligence*, 43(7):2480–2495, 2020.

Yulun Zhang, Kunpeng Li, Kai Li, Gan Sun, Yu Kong, and Yun Fu. Accurate and fast image denoising via attention guided scaling. *IEEE Transactions on Image Processing*, 30:6255–6265, 2021c.

Zunjin Zhao, Bangshu Xiong, Lei Wang, Qiaofeng Ou, Lei Yu, and Fa Kuang. Retinexdip: A unified deep framework for low-light image enhancement. *IEEE Transactions on Circuits and Systems for Video Technology*, 32(3):1076–1088, 2021.

Man Zhou, Xueyang Fu, Jie Huang, Feng Zhao, Aiping Liu, and Rujing Wang. Effective pan-sharpening with transformer and invertible neural network. *IEEE Transactions on Geoscience and Remote Sensing*, 60:1–15, 2021.

Man Zhou, Xueyang Fu, Jie Huang, Feng Zhao, Aiping Liu, and Rujing Wang. Effective pan-sharpening with transformer and invertible neural network. *IEEE Transactions on Geoscience and Remote Sensing*, 60:1–15, 2022a. doi: 10.1109/TGRS.2021.3137967.

Man Zhou, Keyu Yan, Jie Huang, Zihe Yang, Xueyang Fu, and Feng Zhao. Mutual information-driven pan-sharpening. In *Proceedings of the IEEE/CVF Conference on Computer Vision and Pattern Recognition*, pp. 1798–1808, 2022b.

Appendix

In this appendix, we provide additional details and results. In Sec. A, we present further discussion on our motivation. In Sec. B, we present the discussion on the reason of our effectiveness. In Sec. C, we show more comparison results between our method and existing methods on multiple image restoration tasks.

A Motivation

Referring to the previous works. As pointed out in Oppenheim et al. (1979), the motivation comes from a well-known property of the Fourier transformation: the Fourier phase spectrum preserves high-level semantics, while the amplitude spectrum contains low-level features. From Xu et al. (2021a), the amplitude and phase components of Fourier space correspond to the style and semantic information of an image.

Motivation on image enhancement. From Xu et al. (2021a), the amplitude and phase components of Fourier space correspond to the style and semantic information of an image. This property can be extended in exposure correction: the amplitude component of an image reflects the lightness representation while the phase component corresponds to structures and is less related to lightness. As shown in Fig. 5, we first swap the amplitude and phase components of different exposures of the same context. More visual clues can refer to Fig. 6 The recombined result of the amplitude of underexposure and the phase of over-exposure has similar lightness appearance with underexposure, while the other behaves conversely. This implies that the swapped amplitude contains most lightness information while the phase component corresponds to the structure representation and is less affected by lightness.

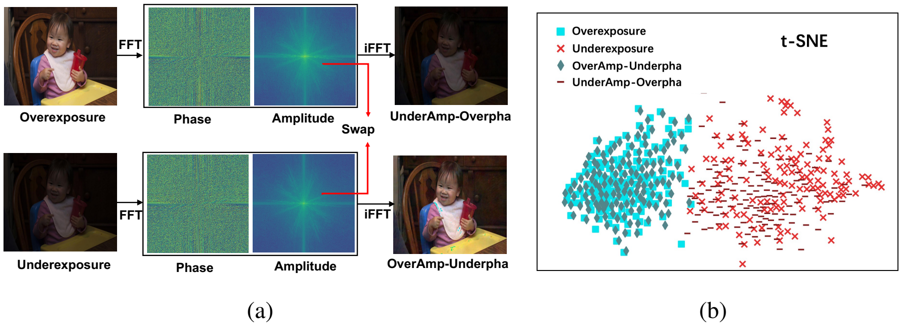

Figure 5: **(a) We swap the amplitude and phase components of different exposures of the same context.** The recombined result of the amplitude of underexposure and the phase of over-exposure (UnderAmp-Overpha) has similar lightness appearance with underexposure, while the recombined result of the amplitude of overexposure and the phase of underexposure (OverAmp-Underpha) has similar lightness appearance with overexposure. **(b) The t-SNE for images of over-exposure, underexposure, UnderAmp-Overpha, and OverAmp-Underpha.** The distributions of images in UnderAmp-Overpha and Underexposure are matched, while the distributions of images in OverAmp-Underpha and Overexposure are matched. (b) indicates that the swapped amplitude contains most lightness information.

To further validate our observation, as shown in Fig. 7, we apply the inverse Fast Fourier Transform (iFFT) to the phase and amplitude components to visualize them in spatial domain. The appearance of the phase representation is more similar with the structure representation, and the distribution of the phase component is less affected by lightness. To this end, the phase component is more related to structures that are less affected by lightness in spatial domain.

Motivation on image de-raining. Fourier transformation: the Fourier phase spectrum preserves high-level semantics, while the amplitude spectrum contains low-level features Oppenheim et al. (1979). Fig. 8 shows the results of swapping the Fourier amplitude and phase spectrum of rainy/clean images. For the images with or without same content, most rain streaks information

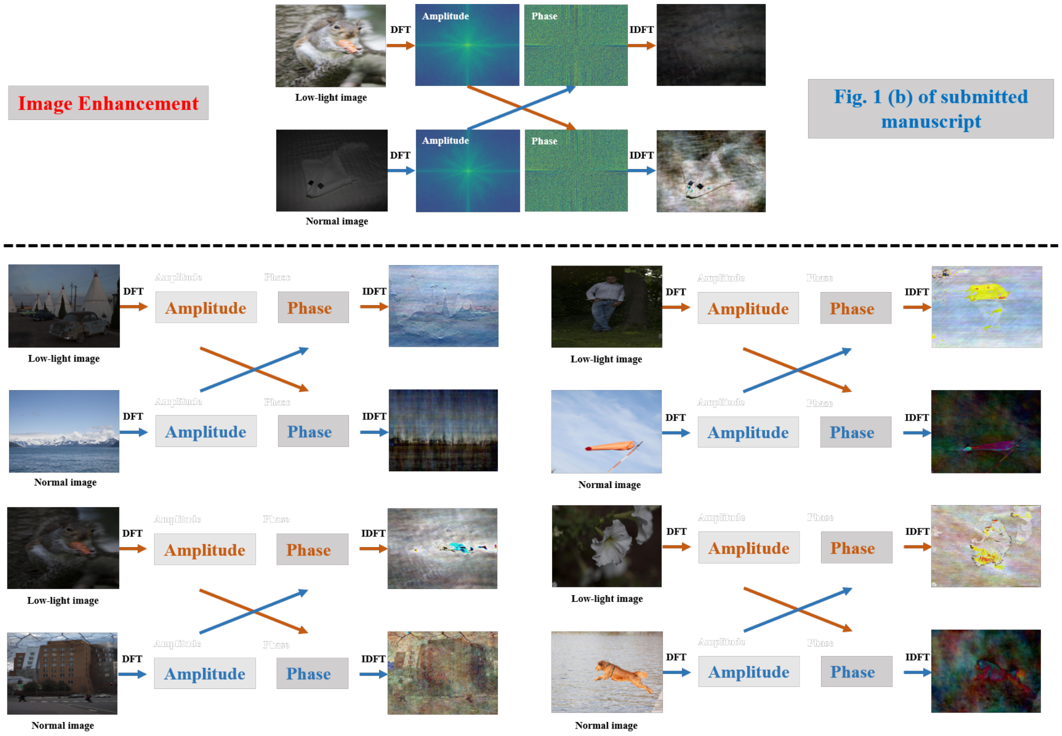

Figure 6: Analysis of discrete Fourier transform (DFT) for low-light image enhancement task. In detail, we swap the amplitude and phase components of the degraded image and a clear version with same or different contents. It can be observed that the degradation effect is transferred with the swapping of amplitude component, indicating that Fourier transform is capable of disentangling image degradation and content component and the degradation mainly lies in the amplitude component. This motivates us to leverage Fourier transform as the image degradation prior embedded into image restoration framework.

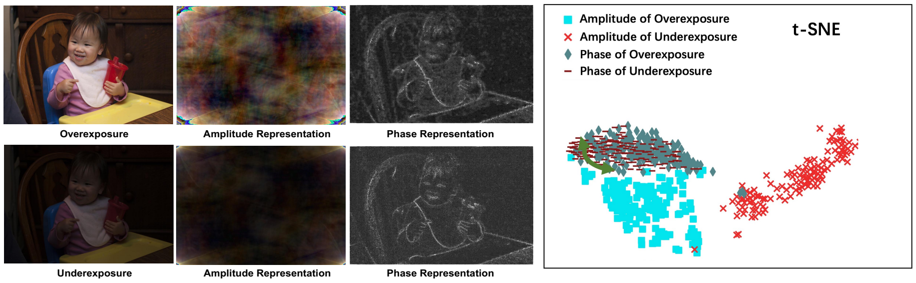

(a) (b)

Figure 7: **(a) Visualization of the amplitude and phase components of an image with the same context but different exposures.** We apply the iFFT to the phase and amplitude to compare the phase and amplitude in spatial domain. The amplitude representation significantly differs between different exposures, while the phase representation is very similar across exposures and represents structure representation. **(b) The t-SNE of amplitude and phase of different exposures.** The distributions of phase representations across different exposures are matched, while distributions of amplitude representations across different exposures vary greatly. It means the phase component contains most structure information and is less affected by lightness.

is preserved in the amplitude spectrum of rainy images. This indicates that the phase of rainy im-

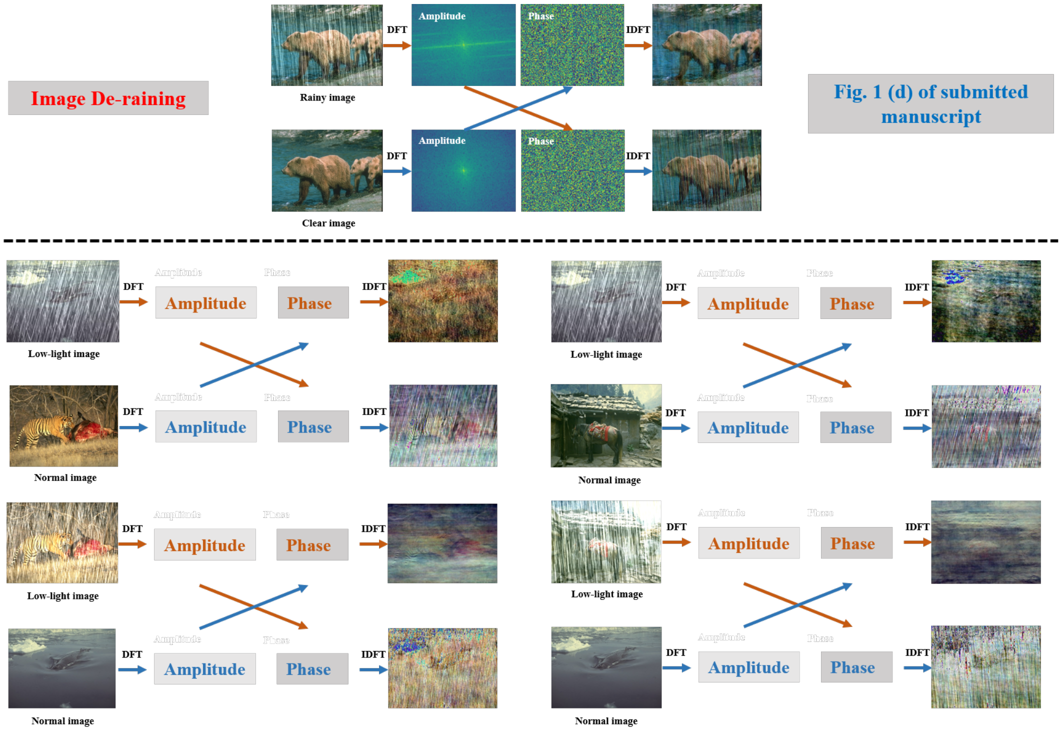

Figure 8: Analysis of discrete Fourier transform (DFT) for image de-raining task. In detail, we swap the amplitude and phase components of the degraded image and the clear version with or without same content. It can be observed that the degradation effect is transferred with the swapping of amplitude component, indicating that Fourier transform is capable of disentangling image degradation and content component and the degradation mainly lies in the amplitude component.

ages keeps the similar background structures as the ground truth. In this way, the Fourier prior is achieved by learning the transformation of the amplitude and phase spectrum separately.

B Discussion on the reason of our effectiveness

Image restoration is essentially an ill-posed optimization problem. For traditional image restoration algorithms, the common sense is to explore the intrinsic knowledge and image prior to constraint the solution space and thus obtain good solution. Besides, the effectiveness of global modeling for image restoration has been demonstrated in existing works. In our work, our proposed framework incorporates both advantages of global modeling and general image degradation prior that are introduced by Fourier transformation, thus achieving better performance.

Some recent works Dai et al. (2022); Yu et al. (2022) have confirmed that the "spatial interaction + channel evolution" is the core contribution of effectiveness within transformer. Our work stands on the principle with new designs in Fourier space, thus achieving better results.

Image restoration aims to remove the degradation effect and restore clear image. It can be treated as image filtering process. In our work, we conduct extensive analysis in Fourier space and infer that Fourier transform is capable of disentangling image degradation and content component and the degradation mainly lies in the amplitude component. To this end, our method first transforms the spatial representation in Fourier space with amplitude and phase and then employs the convolution to perform the filtering function over the amplitude and phase, thus achieving the clear reconstruction. The Fourier prior is embedded in above procedure and follows the consistent principle of the frequency filtering that is common in digital image processing. Therefore, it further achieves performance gains.

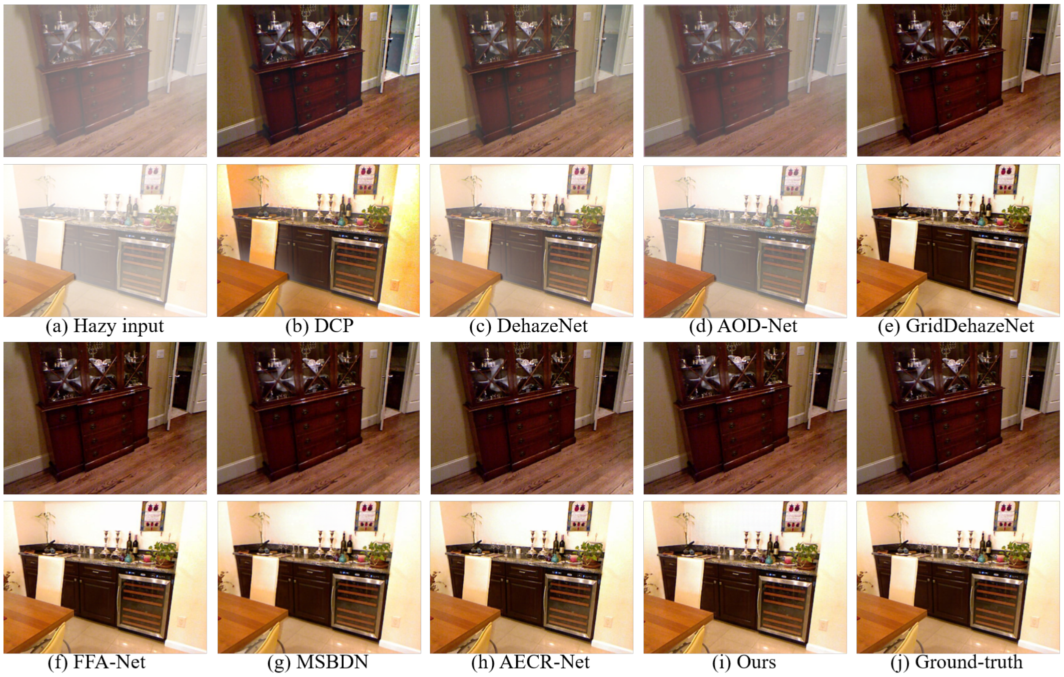
(a) Hazy input (b) DCP (c) DehazeNet (d) AOD-Net (e) GridDehazeNet

(f) FFA-Net (g) MSBDN (h) AECR-Net (i) Ours (j) Ground-truth

Figure 9: The visual comparison on image de-hazing task.

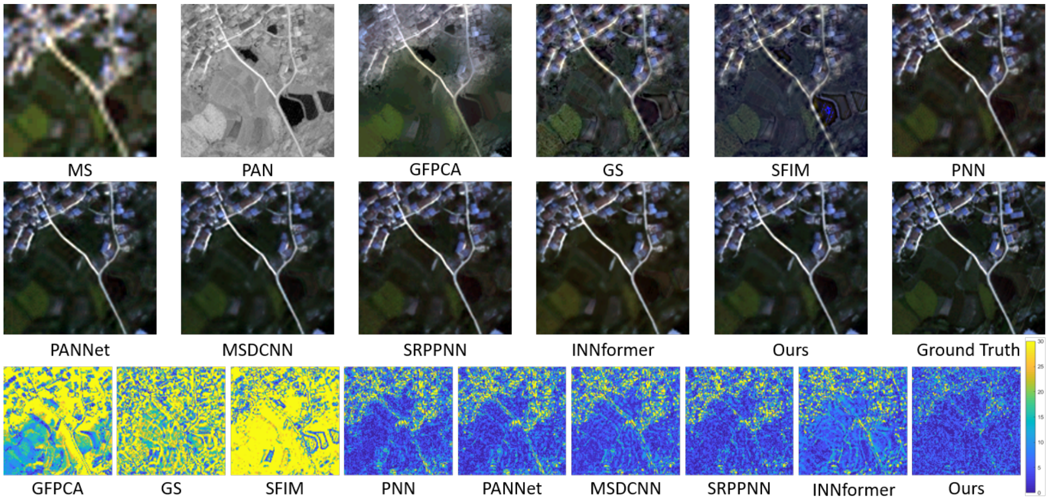

Figure 10: The visual comparison on guided image super-resolution task.

The proposed general image degradation prior is capable of achieving the degradation and content disentanglement, which alleviates the difficulty in network optimization.

C More Comparisons

In this section, we provide more visual comparisons with state-of-the-art methods over the reported tasks. As can be seen in Fig. 9, Fig. 10, Fig. 13, Fig. 14, Fig. 11 and Fig. 12, our proposed method achieves the best performance against other state-of-the-art algorithms.

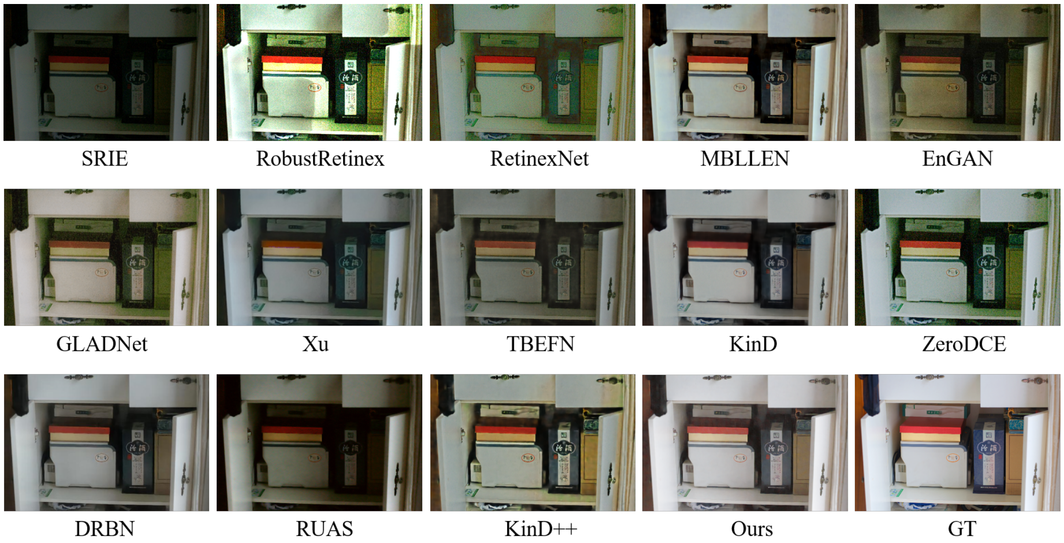

Figure 11: The visual comparison on low-light image enhancement task (LOL dataset).

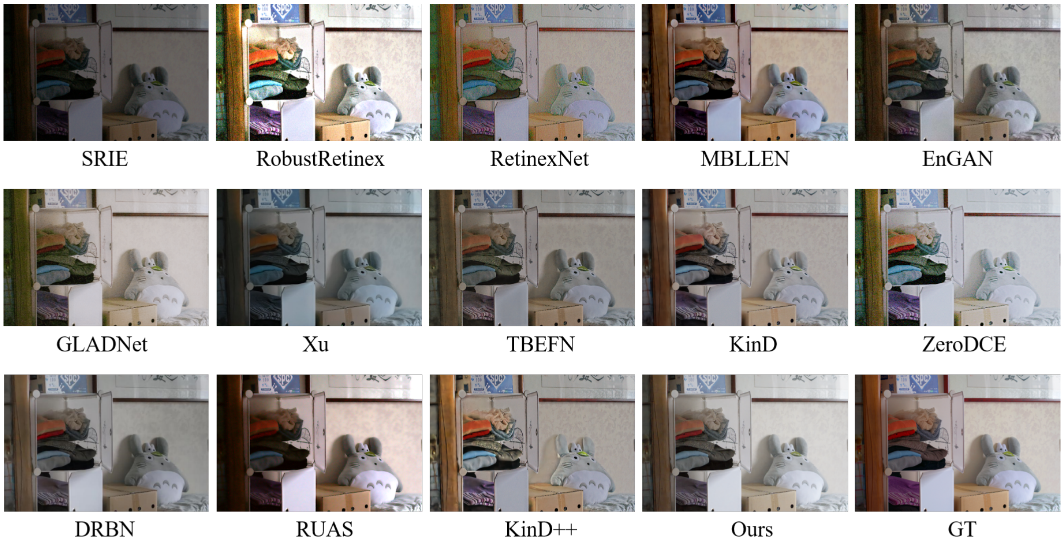

Figure 12: The visual comparison over low-light image enhancement task (LOL dataset).

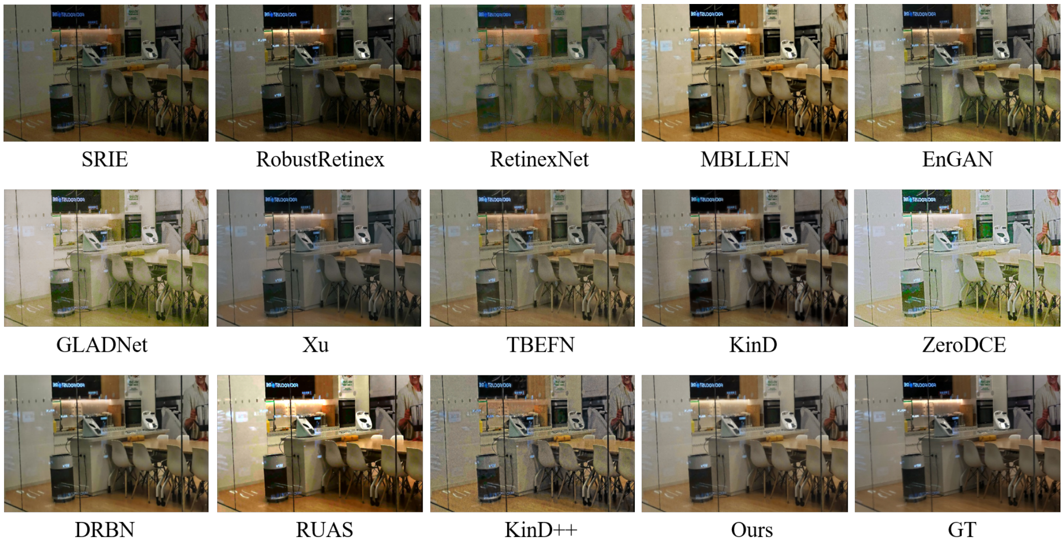

Figure 13: The visual comparison over low-light image enhancement task (Huawei dataset).

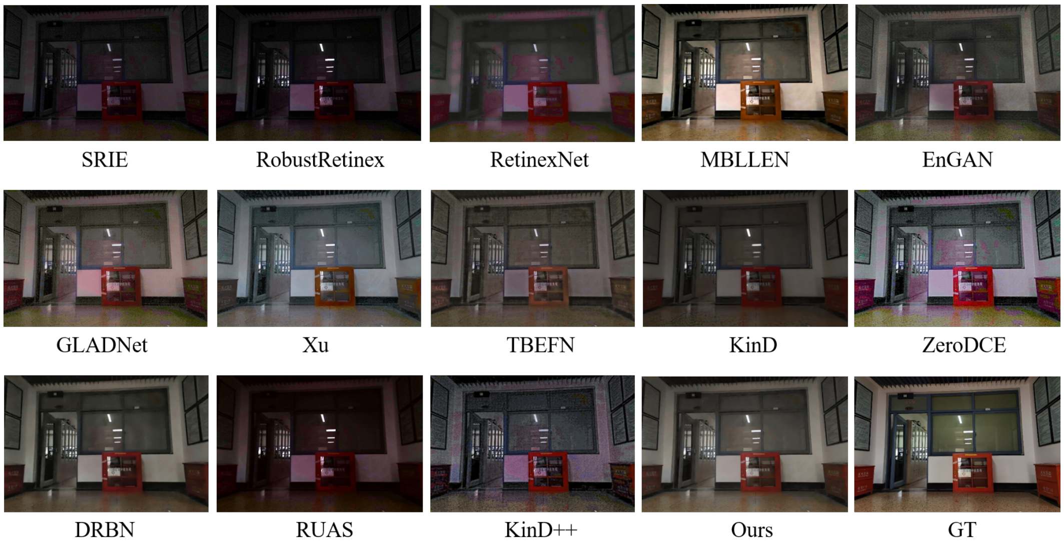

Figure 14: The visual comparison over low-light image enhancement task (Huawei dataset).